Nucleosynthesis driven by Coulomb explosion of nanodroplets

Isidore Last and Joshua Jortner
School of Chemistry, Tel-Aviv University, Ramat Aviv, 69978 Tel-Aviv, Israel

(Received 6 August 2007; accepted 30 October 2007; published online 3 December 2007)

This paper presents a computational and theoretical study of the yields for the $^{12}C(p,\gamma)^{13}N$ and $^{12}C(d,n)^{13}N$ nucleosynthesis reactions driven by high-energy (MeV) Coulomb explosion (CE) of $(CH_4)_n$ and $(CD_4)_n$ nanodroplets ($n=10^4-10^7$, radii $R_0=100-500$ Å) in ultraintense near-infrared Gaussian laser fields (peak intensities $I_M=10^{18}-10^{19}$ W cm^{-2}, pulse length $\tau=25$ fs). Efficient nucleosynthesis with ^{12}C nuclei requires the production of protons and deuterons in the energy range of 0.5–2.0 MeV, which is accomplished by CE of nanodroplets. The energy distributions of the nuclei were obtained from scaled molecular dynamics simulations and were utilized to calculate the energy averaged cross sections and the reaction yields for nucleosynthesis. Two distinct reaction modes were established pertaining to reactions inside the plasma filament volume (IF), and to reactions outside the plasma filament volume (OF). The dominating contribution to the total yields originates from the OF mode. The time resolved γ-ray emission for $^{12}C(p,\gamma)^{13}N$ will be exhibited in distinct time intervals of 2–100 ps for the OF mode and of 65 fs–3 ps for the IF mode. Estimates of the yields were provided by incorporating the effects of nanodroplet size distributions that result in a slow size dependence of the yields in the range $R_0>250$ Å, and the effects of laser intensity attenuation in an assembly of nanodroplets that result in the decrease of the OF and IF yields due to the decrease of the effective plasma filament volume. For 400 Å nanodroplets at $I_M=4\times10^{18}-10^{19}$ W cm^{-2}, under realistic experimental conditions, the $^{12}C(p,\gamma)^{13}N$ nucleosynthesis driven by CE of $(CH_4)_n$ nanodroplets is characterized by a yield (per laser pulse) of ~100, while the yield for the $^{12}C(d,n)^{13}N$ nucleosynthesis driven by CE of $(CD_4)_n$ clusters is $\sim9\times10^4$. Table-top nucleosynthesis driven by nanodroplet CE is amenable to experimental observation. © *2007 American Institute of Physics*. [DOI: 10.1063/1.2815792]

I. INTRODUCTION

The response of elemental and molecular clusters to ultraintense (peak intensity $I_M=10^{15}-10^{21}$ W cm^{-2}), ultrafast (temporal length $\tau=10-100$ fs) laser pulses drives attosecond-femtosecond electron dynamics of sequential-parallel inner ionization, nanoplasma formation, and outer ionization of the nanoplasma.[1–3] Concurrently and in parallel with outer ionization, nuclear dynamics of Coulomb explosion (CE) sets in (on the time scale of 10–100 fs), with the production of high-energy (1 keV–1 MeV), highly charged ions and nuclei.[2,3] The energies of the ions or nuclei produced by cluster CE increase with increasing the cluster size, as shown experimentally,[4–10] demonstrated by molecular dynamics (MD) simulations,[11–16] and established theoretically with the advent of scaling laws for CE energetics.[6,17–19] Important applications of high-energy CE for nuclei pertain to tabletop dd $^2D(d,n)^3He$ fusion driven by CE of deuterium containing clusters[6,8,11,20–23] and to nucleosynthesis of p+A reactions (A=$^{12}C^{6+}$, $^{14}N^{7+}$, and $^{16}O^{8+}$) driven by CE of large clusters of $(CH_4)_n$, $(NH_3)_n$ and $(H_2O)_n$,[24] which is of interest in nuclear astrophysics.[25] In what follows we shall refer to a large cluster with $R_0\geq100$ Å (10 nm) as a nanodroplet. The realization of efficient nucleosynthesis driven by nanodroplet CE will be achieved under the following conditions:

(1) Production of nuclear matter. Complete inner and outer nanodroplet ionizations are required to produce "bare" nuclear matter of protons and nuclei (or protons and highly charged heavy ions).

(2) Extreme inner ionization. The laser intensity (characterized by the peak intensity I_M) has to be sufficiently high to allow for the formation of bare nuclei by inner ionization. For a single CH_4 molecule, this can be realized for $I_M>4\times10^{19}$ W cm^{-2}. For nanodroplets, the intensity corresponding to a complete stripping of a molecule is reduced relative to the single atom value, due to the ignition effect, which originates from the contribution of the ions to the inner field that drives barrier suppression ionization.[2,3,26]

(3) Complete outer ionization. Complete outer ionization of the nanoplasma electrons will be realized at a laser peak intensity of I_M for a cluster radius of $R_0\leq R_0^{(I)}$, where $R_0^{(I)}$ is the border radius for complete cluster outer ionization,[12,14] which is referred to as cluster vertical ionization (CVI). The intensity dependence of the border radius is[12,14] $R_0^{(I)}\propto I_M^{1/2}$. At very high, but accessible, intensities of $I_M(=10^{20}$ W cm$^{-2})$, the largest cluster (nanodroplet) sizes undergoing CVI fall in the range of $R_0=350-750$ Å (with $R_0<R_0^{(I)}$),[24] which is amenable to experimental preparation.

(4) Attainment of ultrahigh CE energies. The maximization of the yields of p+A nucleosynthesis will be achieved at high center of mass energies (E) of the nuclei, where the cross sections[25] attain their highest values; i.e., $E\simeq400$ keV for the $^{12}C^{6+}(p,\gamma)^{13}N^{7+}$ reaction (Fig. 1), and $E>1$ MeV for the $^{14}N(p,\gamma)^{15}O$ and $^{16}O(p,\gamma)^{17}F$ reactions.[25] The cluster size dependence of the kinetic

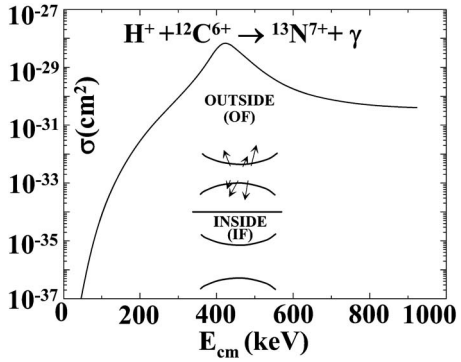

FIG. 1. Dependence of the cross sections for $^{12}C(p,\gamma)^{13}N$ on the center of mass energy [calculated from $\sigma(E^H, E^C=0)$ data (Ref. 30)]. The insets schematically portray the plasma filament with boundaries represented by solid lines. The IF reaction mode involves collisions of nuclei within the plasma filament, while the OF reaction mode involves nuclei-cluster collisions outside the plasma filament.

energies of the nuclei requires the utilization of large "bare" nanodroplets of nuclear matter. The nanoparticle size dependence of the maximal energies E_M and the average energies E_{av} for ions from CE in the CVI domain ($R_0 \leq R_0^{(I)}$) is given by the divergent scaling law $E_{av}, E_M \propto R_0^2$. CE of nanodroplets in the size domain $R_0 \simeq R_0^{(I)}$ (point 3) will result in kinetic energies of $\sim$30 MeV for C^{6+}, N^{7+}, and O^{8+} nuclei, and of $\sim$3 MeV for protons, which are required to drive efficient nucleosynthesis (point 1). We note in passing that a further increase of R_0 brings the system to the non-CVI domain ($R_0 > R_0^{(I)}$), where the increase of E_M and E_{av} with increasing R_0 is slowed down and the ion energy becomes significantly dependent on the laser intensity.

Recently, we used[24] a simplified picture for inner/outer nanodroplet ionization, in conjunction with an electrostatic model for the energetics of CE of nanodroplets, to estimate the yields for p+A reactions. In this paper we present a theoretical and computational study of the $^{12}C(p,\gamma)^{13}N$ nucleosynthesis reaction driven by CE of methane clusters. The large nanodroplet sizes (containing $\sim 10^5-10^7$ atoms), for which CE drives efficient nucleosynthesis, preclude the use of the traditional particle MD simulation methods. We utilized a scaling procedure for MD simulations recently suggested by Petrov *et al.*[27] and developed by us,[16] which allows for the computations of extreme cluster ionization levels for multielectron dynamics and CE energetics in nanodroplets. This scaling procedure for MD will provide new information for the γ-ray yields in the $^{12}C(p,\gamma)^{13}N$ nucleosynthesis driven by CE of $(CH_4)_n$ nanodroplets. We performed estimates of the nucleosynthesis yields under real-life conditions, incorporating the effects of nanoparticle size distribution on the CE energy distribution, and of the attenuation of the laser intensity in an assembly of nanoparticles. The same computational methods will also be applied for the evaluation of neutron yields for the $^{12}C(d,n)^{13}N$ fusion reaction, for which experimental data on surfaces have become available.[28]

II. THE $^{12}C(p,\gamma)^{13}N$ NUCLEOSYNTHESIS REACTION DRIVEN BY CE OF METHANE NANODROPLETS

A. Nucleosynthesis reactions inside and outside the plasma filament

We consider the $^{12}C(p,\gamma)^{13}N$ nucleosynthesis reaction induced by the collision of two energetic nuclei, i.e., Z_1 and Z_2, generated by CE of molecular nanoparticles, whose constituent molecules contain these nuclei. The high-energy nuclei and heavy ions are generated inside a restricted laser focus volume, V_f, where the uniform plasma filament is formed, whereas the ionization of clusters outside this volume can be ignored.[29] Two distinct nucleosynthesis reaction modes driven by CE of nanodroplets will be established, pertaining to reactions within the laser focal volume and outside of it. Nucleosynthesis reactions take place both inside the plasma filament (IF), where collisions between high-energy nuclei produced from CE of different clusters occur,[6,8,21,29] and outside the plasma filament (OF), where the high-energy nuclei from the plasma filament collide with nuclei within clusters located in the cluster beam outside the filament.[22] The IF and OF reactions are schematically presented in the inset to Fig. 1. The total reaction yield (per laser pulse) is

$$Y_{tot} = Y_{IF} + Y_{OF} \tag{1}$$

with the Y_{IF} and Y_{OF} yields for the IF and OF reactions, respectively, being determined for heteronuclear collisions by the equation[24]

$$Y = k_1 k_2 \rho_{mol}^2 V_f \ell \langle\sigma\rangle, \tag{2}$$

where k_1 and k_2 are the number of reagent atoms in a molecule, ρ_{mol} is the molecular density within the relevant reaction volume, ℓ is the reaction path length, and $\langle\sigma\rangle$ is the reaction cross section averaged over the energy distribution of the reactants. The attributes ℓ and $\langle\sigma\rangle$ are different for the Y_{IF} and Y_{OF} components. It is important to note that highly charged atomic ions (e.g., C^{q+}, $q<6$) with sufficiently high energies may also contribute to the reaction yield in the same way as bare nuclei since the bound energy of atomic electrons is much lower than the collision energy of reactants.

The reaction path length in the IF mode (ℓ_{IF}) is of the order of the plasma filament radius (r_f).[6] In our work, we take it as $\ell_{IF}=1.6r_f$.[11] The reaction path length of the OF mode ℓ_{OF} is equal to the cluster beam radius R_{beam} (for $R_{beam} \gg r_f$), provided that the energy losses of the high-energy particles along the path $\ell_{OF}=R_{beam}$ are small. The geometric parameters in Eq. (2) will now be specified. The laser filament volume, where the high-energy nuclei and heavy ions are formed, is taken as $V_f=5\times10^{-7}$ cm^3,[24] with a filament radius of $r_f=0.002$ cm. The low values of these geometric parameters are due to the ultrahigh intensity employed herein ($I_M=10^{18}-10^{19}$ W cm^{-2}).[2,6,22] Thus, $\ell_{IF}=0.003$ cm, while $\ell_{OF}=R_{beam}=0.1$ cm. Finally, we take $\rho_{mol}=4\times10^{18}$ cm^{-3}.[24]

For the $^{12}C(p,\gamma)^{13}N$ reaction (Z_1=p, $Z_2=^{12}C$) generated by CE of methane clusters, the coefficients in Eq. (3) are $k_1=4$ and $k_2=1$. In the IF mode for the reaction $p(E^H) + ^{12}C(E^C)$,

$$\langle\sigma\rangle_{\mathrm{IF}} = \frac{1}{2}\int_0^{E_M^{\mathrm{H}}} P(E^{\mathrm{H}})\mathrm{d}E^{\mathrm{H}} \int_0^{E_M^{\mathrm{C}}} P(E^{\mathrm{C}})\mathrm{d}E^{\mathrm{C}} \times \int_0^{\pi} \sigma(E_{\mathrm{cm}})\sin\alpha \mathrm{d}\alpha, \quad (3)$$

where E^{H} and E^{C} are the laboratory frame energies of protons and of C^{q+} ions, respectively, $P(E^{\mathrm{H}})$ and $P(E^{\mathrm{C}})$ are their energy distributions, E_M^{H} and E_M^{C} are energy maxima, α is the collision angle, and E_{cm} is the center of mass energy,

$$E_{\mathrm{cm}} = \mu[E^{\mathrm{H}}/m_{\mathrm{H}} + E^{\mathrm{C}}/m_{\mathrm{C}} - 2(E^{\mathrm{H}}E^{\mathrm{C}}/m_{\mathrm{H}}m_{\mathrm{C}})^{1/2}\cos\alpha] \quad (4)$$

with $m_{\mathrm{H}}=1$, $m_{\mathrm{C}}=12$, and the reduced mass $\mu=0.923$. In the OF mode, the average reaction cross section is reduced to the sum of two one-dimensional integrals representing the collisions, i.e., $\mathrm{p}(E^{\mathrm{H}}>0)+{}^{12}\mathrm{C}(E^{\mathrm{C}}=0)$ and ${}^{12}\mathrm{C}(E^{\mathrm{C}}>0)+\mathrm{p}(E^{\mathrm{H}}=0)$, so that

$$\langle\sigma\rangle_{\mathrm{OF}} = \int_0^{E_M^{\mathrm{H}}} P(E^{\mathrm{H}})\sigma(E_{\mathrm{cm}}^{\mathrm{H}})\mathrm{d}E^{\mathrm{H}} + \int_0^{E_M^{\mathrm{C}}} P(E^{\mathrm{C}})\sigma(E_{\mathrm{cm}}^{\mathrm{C}})\mathrm{d}E^{\mathrm{C}}. \quad (5)$$

The center of mass energies in Eq. (5) are

$$E_{\mathrm{cm}}^{\mathrm{H}} = \frac{m_{\mathrm{C}}}{m_{\mathrm{H}}+m_{\mathrm{C}}}E^{\mathrm{H}}, \quad (6a)$$

and

$$E_{\mathrm{cm}}^{\mathrm{C}} = \frac{m_{\mathrm{H}}}{m_{\mathrm{H}}+m_{\mathrm{C}}}E^{\mathrm{C}}. \quad (6b)$$

The dependence of the cross section $\sigma(E_{\mathrm{cm}})$ on the center of mass energy E_{cm}, presented in Fig. 1, was derived from the $\sigma(E^{\mathrm{H}},E^{\mathrm{C}}=0)$ data[30] by using Eq. (6a). The reaction cross section exhibits a sharp resonance with a maximum at $E_{\mathrm{cm}}\approx 420$ keV. The optimal interval, providing relatively large reaction cross sections, i.e., $\sigma\sim 10^{-29}-10^{-28}$ cm^2, lies in the vicinity of this maximum in the range $E_{\mathrm{cm}}\approx 370-510$ keV. In the OF mode the optimal energy interval corresponds, according to Eqs. (6a) and (6b), to the laboratory frame energies $E^{\mathrm{H}}\approx 400-550$ keV and $E^{\mathrm{C}}\approx 4.8-6.6$ MeV. In the IF mode for the front collisions, $\alpha=180°$, the optimal laboratory frame energies lie, according to Eq. (4), inside the intervals determined by the condition

$$400\ \mathrm{keV} < [(E^{\mathrm{H}}/m_{\mathrm{H}})^{1/2} + (E^{\mathrm{C}}/m_{\mathrm{C}})^{1/2}]^2 < 550\ \mathrm{keV}. \quad (7)$$

The calculation of the reaction cross sections $\langle\sigma\rangle$ averaged over the energy distribution of the reactants (nuclei or heavy ions) for the IF mode [Eq. (3)] and for the OF mode [Eq. (5)] requires the simulation of the energy distributions $P(E^{\mathrm{H}})$ and $P(E^{\mathrm{C}})$ in CE of the parent cluster. The kinetic energy distribution $P(E)$ for nuclei and ions from CE of clusters qualitatively differs from the thermal energy distribution $P_{\mathrm{thermal}}(E)\propto E^{1/2}\exp(-\beta E)$ in the following features. (1) $P_{\mathrm{thermal}}(E)$ is characterized by a long, high-energy tail, while $P(E)$ is restricted in the range $E\leq E_M$, with E_M being close to E_{av}. (2) In CE of heteroclusters, e.g., $(CH_4)_n$, the energies of the heavy nuclei or ions are larger by a numerical factor of 4–6 than the protons, due to charge effects.[11] Thus, the energetic carbon nuclei and ions may also contribute to the ${}^{12}\mathrm{C}(\mathrm{p},\gamma){}^{13}\mathrm{N}$ reaction yields; while in thermal equilibrium, only the high-energy protons contribute to this reaction. Since the values of the $(E^{\mathrm{H}}/m_{\mathrm{H}})^{1/2}$ and $(E^{\mathrm{C}}/m_{\mathrm{C}})^{1/2}$ terms in the inequality (7) are expected to be close to each other, the efficient reaction cross section in the IF mode can be reached at lower ion energies than in the OF mode.

B. A scaling procedure for the simulations

Data for the kinetic energy distributions $P(E)$ of the CE product nuclei and heavy ions were obtained from simulations of scaled electron and ion dynamics (SEID) for nanodroplets driven by ultraintense lasers. The SEID considers MD in a scaled cluster with a reduced number of composite particles (pseudoelectrons and pseudo-ions/nuclei), scaled initial interparticle distances and scaled short-range potential parameters.[16] The conditions for the accuracy of the SEID method rest on the realization of nearly identical accelerations and trajectories of the cluster particles and of the composite particles within the scaled cluster. In the SEID procedure, a single scaling parameter s is used for the composition, mass, and charge of all pseudoparticles. The initial distances between the pseudoparticles are scaled by $s^{1/3}$. The scaled molecule of the scaled methane cluster consists of five heavy pseudoparticles (HPPs), i.e., one carbon pseudoparticle $\tilde{\mathrm{C}}$ with mass $\tilde{m}_{\mathrm{C}}=sm_{\mathrm{C}}$, separated initially from the pseudoparticle $\tilde{\mathrm{C}}$ by the distance $\tilde{r}_{\mathrm{C-H}}=s^{1/3}r_{\mathrm{C-H}}$, with $r_{\mathrm{C-H}}$ being the C–H distance in the CH_4 molecule. In accordance with the standard simulations, where each cluster atom at the onset of the SEID simulations is singly ionized,[26] the initial HPP charges are $\tilde{q}_{\mathrm{C}}=\tilde{q}_{\mathrm{H}}=se$. In the vicinity of each HPP, a light pseudoparticle (LPP) with mass $\tilde{m}_e=sm_e$ and charge $\tilde{q}_e=-se$ is located at distance $\tilde{r}_b=s^{1/3}r_b$, r_b being the barrier suppression ionization distance.[16] The neighboring carbon HPPs, $\tilde{\mathrm{C}}$, are initially separated from each other by the distance $\tilde{r}_{\mathrm{C-C}}=s^{1/3}r_{\mathrm{C-C}}$, with $r_{\mathrm{C-C}}$ being the C–C distances in the neutral cluster. The number $\tilde{n}$ of scaled molecules in the scaled $(\tilde{\mathrm{C}}\tilde{\mathrm{H}}_4)_{\tilde{n}}$ cluster is determined as the closest integer to the value n/s, with n being the number of molecules in the real $(CH_4)_n$ cluster. The radius $\tilde{R}_0$ of the scaled cluster is close to the real cluster radius R_0, if the condition $\tilde{n}\gg 1$ is fulfilled. After the scaled cluster is constructed in its initial structure, the standard MD simulation procedure for the pseudoparticle is applied.

C. Energy distribution and averaged cross sections

In cluster CE experiments the cluster beam consists of different size clusters.[7,8,31,32] Consequently, the energy distributions produced in the plasma filament ions have to be determined by averaging over the cluster size distribution $\Pi(R_0)$,

$$\bar{P}(E^J) = \int_0^{\infty} \Pi(R_0)P(E^J;R_0)\mathrm{d}R_0, \quad (8)$$

where $P(E^J;R_0)$ is the energy distribution of ions J (=H,C) produced by a single cluster of radius R_0. The spatial disper-

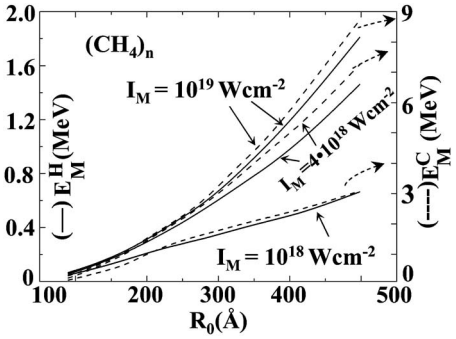

FIG. 2. Nanoparticle size dependence of the maximal energies of $H^+(E_M^H)$ and of $C^{6+}(E_M^C)$ in the CE of $(CH_4)_n$ nanodroplets. The laser peak intensities are marked on the curves.

sion of the laser intensity I_M inside the plasma filament[32] will be ignored. We use the log-normal size distribution[8]

$$\Pi(R_0) = \frac{1}{(2\pi)^{1/2}\sigma_R R_0} \exp\left[-\left(\frac{\ln(R_0/R_{\rm av}) + \sigma_R^2/2}{2^{1/2}\sigma_R}\right)^2\right], \tag{9}$$

where $R_{\rm av}$ is the average cluster radius and σ_R is the dispersion width of the cluster radius R_0, which is related to the dispersion of the width of the cluster molecule number n by $\sigma_R=\sigma_n/3$. In this work we take the size dispersion width $\sigma_n=1$ ($\sigma_R=0.333$),[8] for the size averaged energy distributions [Eq. (8)]. Replacing $P(E^{\rm H})$ and $P(E^{\rm C})$ in Eqs. (3) and (5) by $\bar{P}(E^{\rm C})$ and $\bar{P}(E^{\rm H})$ [Eq. (8)] results in the cluster size averaged cross sections for the IF and OF modes.

In order to calculate the $^{12}C(p,\gamma)^{13}N$ reaction cross sections and yields, we performed the SEID simulations for methane clusters $(CH_4)_n$ in the size domain $R_0=90-500$ Å ($n=8\times10^4-9\times10^6$). We are using a near-infrared Gaussian laser pulse with light frequency $\nu=0.35$ fs^{-1} (photon energy 1.44 eV) and temporal pulse width $\tau=25$ fs. The peak intensities were $I_M=10^{18}$, 4×10^{18}, and 10^{19} W cm^{-2}, for which the CVI border radii are $R_0^{(I)}=111$, 190, and 270 Å, respectively. At the lowest intensity of $I_M=10^{18}$ W cm^{-2}, all of the clusters treated by us, except for the smallest one, belong to the non-CVI ionization domain, whereas at the two other peak intensities the CVI border lies inside our cluster size domain. In Fig. 2 we present the size dependence of the maximal energies E_M.

The size dependence of $E_M(R_0)$ is affected first of all by the transition at $R_0\sim R_0^{(I)}$ from the CVI to the non-CVI behavior and, in the case of a fixed ion charge, from the CVI $E_M\propto R_0^2$ dependence to the roughly linear E_M increase with R_0 at $R_0\gg R_0^{(I)}$.[24] Such a size dependence of $E_M(R_0)$ may be complicated by the energy increase due to the increase of the charge of the carbon ion C^{q+} with increasing R_0, which is due to the ignition effect. The most complicated behavior is exhibited at the intensity $I_M=10^{18}$ W cm^{-2}, when the average carbon charge increases from $q=4$ for $R_0=90$ Å to $q=5.8-5.96$ in the interval $R_0=285-498$ Å.

The maximal energies E_M for the efficient reaction in the OF mode, i.e., $E^{\rm H}\approx400-550$ keV and $E^{\rm C}\approx4.8-6.6$ MeV (see Sec. II A), are provided by clusters with $R_0\sim400$, 260,

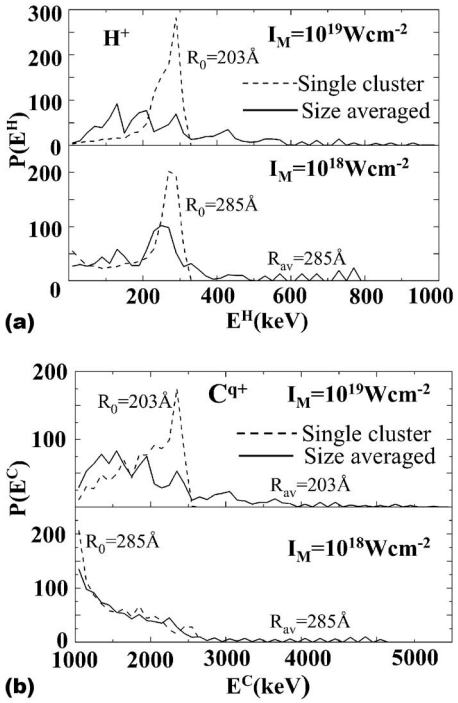

FIG. 3. Distributions of kinetic energies of protons (a) and C^{6+} nuclei (b) in the CE of $(CH_4)_n$ nanodroplets at $I_M=10^{18}$ W cm^{-2} and 10^{19} W cm^{-2} (marked on the panels). The single nanodroplet size R_0 and averaged size $R_{\rm av}$ are marked on the curves.

and 250 Å for $I_M=10^{18}$, 4×10^{18}, and 10^{19} W cm^{-2}, respectively (Fig. 2). The reaction efficiency, however, is determined not only by the maximal energy E_M but also by the shape of the energy distribution, and particularly by the ion fractions in the vicinity of the E_M energy. Two single cluster energy distributions with similar E_M values are shown in Fig. 3. One of these distributions, for the $R_0=203$ Å cluster at $I_M=10^{19}$ W cm^{-2}, belongs to the CVI domain, whereas the second one, for the $R_0=285$ Å cluster at $I_M=10^{18}$ W cm^{-2}, corresponds to the non-CVI domain with $R_0>R_0^{(I)}$. In the CVI case, the energy distributions $P(E^{\rm H})$ and $P(E^{\rm C})$ for a single cluster size reveal large high-energy maxima in the vicinity of E_M. This feature, which originates from kinematic effects,[11,12] is favorable for enhancement of the reaction efficiency, at least for energies lower than the reaction cross-section peak (Fig. 1). In the non-CVI case, the $P(E^{\rm H})$ distribution reveals not only the high-energy maximum, which is lower and broader than in the CVI case, but also a low-energy ($E^{\rm H}\sim0$) maximum. The differences between the two energy distributions indicate the decrease of the fraction of high-energy protons and carbon ions in the non-CVI domain as compared to the CVI domain.

In Fig. 3, along with the single cluster energy distributions, we also present the energy distributions $\bar{P}(E^{\rm H})$ and $\bar{P}(E^{\rm C})$ averaged over the cluster sizes for the size dispersion width $\sigma_n=1$, and for the averaged cluster radii $R_{\rm av}$, which are equal to the single cluster radii of Fig. 3. The size averaged energy distributions, in contrast to the single clusters, have long high-energy tails, which resemble the thermal distribution. The oscillations in $\bar{P}(E)$ are of statistical origin. Size averaging results in a marked increase of the maximal energy

$\bar{E}_M^J$ [arbitrarily defined as the energy corresponding to the relative population $n(\bar{E}_M^J)/n(\bar{E}_{\rm av}^J) \simeq 10^{-3}$], as compared to the single cluster value E_M^J (J=H,C). In the CVI regime, e.g., for $I_M=10^{19}$ W cm^{-2} and $R_0=R_{\rm av}=203$ Å, $E_M^{\rm H}=320$ keV and $\bar{E}_M^{\rm H}=980$ keV for the protons [Fig. 3(a)], while $E_M^{\rm C}=1510$ keV and $\bar{E}_M^{\rm C}=4800$ keV for C^{6+} nuclei [Fig. 3(b)]. In the non-CVI domain, i.e., for $I_M=10^{18}$ W cm^{-2} and $R_0=R_{\rm av}=286$ Å, $E_M^{\rm C}=1.8$ MeV and $\bar{E}_M^{\rm C}=4.3$ MeV [Fig. 3(b)].

D. Light absorption by a single nanodroplet

The simulations of cluster ionization are based on the assumption that the laser field inside a cluster is spatially homogeneous. This assumption is violated when the light absorption by the cluster particles (electrons, basically) is sufficiently strong to contribute to the attenuation of the laser intensity along its propagation path inside the cluster. Following the treatment proposed by us for the laser light attenuation in the plasma filament,[33] we consider the attenuation inside a cluster to be unimportant if the energy flow ($E_{\rm fl}$) through the cluster is much larger than the total energy ($E_{\rm tot}$) absorbed by the cluster particles, i.e.,

$$E_{\rm fl} \gg E_{\rm tot}. \tag{10}$$

We present[33] $E_{\rm tot}$ as the total energy of the CE product ions and electrons, and $E_{\rm fl}$ as the laser pulse energy flow through the cluster section area at the pulse peak ($t=0$ in our simulations), which is given by

$$E_{\rm fl} = 2.36 \times 10^{-16} \pi [R(t=0)]^2 \tau I_M. \tag{11}$$

Equation (11) presents the cluster radius $R(t)$ in Å, the pulse width τ in femtoseconds, the peak intensity I_M in W cm^{-2}, and $E_{\rm fl}$ in keV. The simulations provide $E_{\rm tot}$ which, together with $E_{\rm fl}$ [Eq. (11)], allows us to check the validity condition [Eq. (10)]. We suggest to consider moderately weak light attenuation for $E_{\rm fl} > 2E_{\rm tot}$. This condition for small absorption by a single cluster is fulfilled at $I_M \geq 4\times10^{18}$ W cm^{-2} for all methane cluster sizes (R_0=90–500 Å, $n=5\times10^4$–9×10^6) considered herein and for $R_0 \leq 400$ Å at $I_M=10^{18}$ W cm^{-2}.

III. γ-RAY YIELDS FROM THE ^{12}C(p,γ)^{13}N REACTION

A. Single cluster and size averaged data

We calculated the reaction cross sections $\langle\sigma\rangle_{\rm IF}$ and $\langle\sigma\rangle_{\rm OF}$ for single clusters by substituting the energy distributions $P(E^{\rm H})$ and $P(E^{\rm C})$ obtained from SEID simulations into the integrals of Eqs. (3) and (5). The dependence of the velocity averaged cross sections on the cluster radius R_0 for the laser intensities $I_M=10^{18}$, 4×10^{18}, and 10^{19} W cm^{-2} is shown in Figs. 4(a) and 4(b) for the IF and OF modes, respectively. In the size interval of relatively small values of R_0 the cross sections exhibit a steep increase with increasing R_0. In this size interval $\langle\sigma\rangle_{\rm IF}$ significantly exceeds $\langle\sigma\rangle_{\rm OF}$, due to larger center of mass energies [compare Eqs. (4) and (6)]. Both in the IF and in the OF modes, the cross sections for the intensities $I_M=4\times10^{18}$ and 10^{19} W cm^{-2} are close to each other, significantly differing from the cross section at

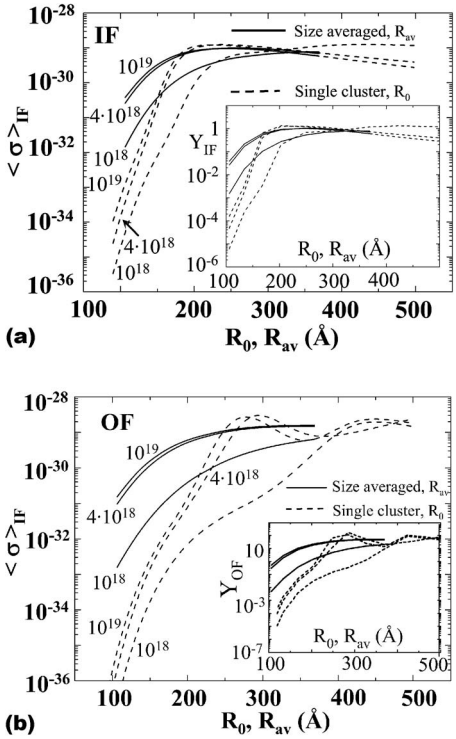

FIG. 4. Energy averaged and size averaged cross sections and ^{12}C(p,γ)^{13}N nucleosynthesis yields per laser pulse (insets) for the ^{12}C(p,γ)^{13}N reaction, in the IF mode (a) and in the OF mode (b). The laser peak intensities (in W cm^{-2}) are marked on the curves. The order of the peak intensities in the insets is identical to those in the main frame.

$I_M=10^{18}$ W cm^{-2}. In the IF mode [Fig. 4(a)], the cross sections $\langle\sigma\rangle_{\rm IF}$ of the two higher intensities reveal a maximum at $R_0 \approx 200$ Å, followed by a very slow decrease. At the lowest intensity of $I_M=10^{18}$ W cm^{-2}, the cross section $\langle\sigma\rangle_{\rm IF}$ does not exhibit any maximum [Fig. 4(a)]. In the OF mode [Fig. 4(b)] the cross sections $\langle\sigma\rangle_{\rm OF}$ of the intensities $I_M \geq 4\times10^{18}$ W cm^{-2} exhibit broad maxima at $R_0 \sim 270$ Å contributed by protons in the optimal energy range of $E^{\rm H} \approx 400$–550 keV (see Sec. II A). $\langle\sigma\rangle_{\rm OF}$ at $I_M=10^{19}$ W cm^{-2} also exhibits the second maximum at $R_0 \approx 430$ Å contributed by carbon ions with the optimal energy of $E^{\rm C} \approx 4.8$–6.6 MeV (see Sec. II A). The maximum in $\langle\sigma\rangle_{\rm OF}$ contributed by protons produced at $I_M=10^{18}$ W cm^{-2} lies near the high end of our R_0 interval. Accidentally, this maximum coincides with the maximum contributed by carbon ions at $I_M=10^{19}$ W cm^{-2}.

The reaction cross sections for energy distributions averaged over the size distribution [Eq. (8)] were calculated from the cross sections for the single-size nanodroplets [Figs. 4(a) and 4(b)]. These size averaged cross sections are presented versus the average nanodroplet radius $R_{\rm av}$ [Figs. 4(a) and 4(b)]. As expected, the dependence of the size averaged cross sections on $R_{\rm av}$ is much flatter than the dependence of the single nanodroplet cross sections on R_0. In the IF mode [Fig. 4(a)], the $\langle\sigma\rangle_{\rm IF}$ cross sections of the size averaged energy distributions exhibit a very broad maxima at $I_M=4\times10^{18}$ and 10^{19} W cm^{-2}. In the OF mode [Fig. 4(b)], the

$\langle\sigma\rangle_{OF}$ cross sections of the size averaged energy distributions do not reveal any maxima, but only some saturation behavior.

The reaction yields for a given experimental condition were evaluated [Eq. (2)] from the cross sections (Fig. 4). The following parameters[24] were used in Eq. (2): $\rho_{mol}=4\times10^{18}$ cm^{-3}, $V_f=5\times10^{-7}$ cm^3, $\ell_{IF}=0.0032$ cm, and $\ell_{OF}=0.1$ cm. Eq. (2) is valid in the OF mode if the energy losses of ions along the ℓ_{OF} path are small (Sec. II A). Because of the lack of data concerning energy losses of the nuclei in methane, we used the data for energy losses of protons in the air,[34] where the energy losses are expected to be somewhat larger than in methane. For the air density of 10^{-4} g cm^{-3}, equal to the methane density of $\rho_{mol}=4\times10^{18}$ cm^{-3}, the $E^H>300$ keV protons, which are mainly responsible for the reaction yield, lose along the path of 0.1 cm less than 2% of their energy. The carbon nuclei energy losses were found by using the Born approximation with appropriate scaling.[35] Since we consider carbon nuclei and protons of the same velocity (the same center of mass energy), the scaling becomes very simple; namely, $\Delta E^C/E^C=(q_C/q_H)^2(m_H/m_C)\Delta E^H/E^H$. According to this relation, the relative energy losses of C^{6+} are only three times larger than for protons, being less than 6%. The energy losses are probably much stronger for C^{q+} ions with $q<6$; however, the fraction of these ions is significant only for the $I_M=10^{18}$ W cm^{-2} intensity when carbon nuclei do not contribute significantly to the reaction. Our estimations allow us to conclude that at $I_M>10^{18}$ W cm^{-2} the energy losses of high-energy particles for ℓ_{OF} of the order of 0.1 cm or less can be neglected.

The yields obtained by us for the IF and OF modes are shown in the insets to Figs. 4(a) and 4(b). The maximal reaction yields for single clusters are of the order of one γ-photon per pulse in the IF mode and 90–160 γ-photons in the OF mode. The present results, based on our SEID simulations, are close to our previous rough estimates performed for a larger laser intensity of $I_M=10^{20}$ W cm^{-2}.[24] The cluster size averaged reaction yields [insets to Figs. 4(a) and 4(b)], like the size averaged cross sections [Figs. 4(a) and 4(b)] demonstrate a relatively flat dependence on the average radius R_{av} for $R_{av}>160$ Å at $I_M\geq4\times10^{18}$ W cm^{-2} and for $R_{av}>250$ Å at $I_M=10^{18}$ W cm^{-2}. The maximal values for the size averaged yields are about one γ-photon per pulse in the IF mode [inset to Fig. 4(a)] and 20–50 γ-photons per pulse in the OF mode [inset to Fig. 4(b)].

B. Attenuation of the laser beam by a cluster assembly

The reaction yields presented in Fig. 4 were obtained for a homogeneous laser intensity inside the plasma filament. The attenuation of the laser beam by the clusters is expected to decrease the nucleosynthesis yield in comparison to the "ideal" conditions of spatial homogeneity of the laser beam. In Sec. II D we showed that light absorption by a single nanoparticle is nearly negligible. However, the laser intensity may decrease along the propagation path due to light absorption by an assembly of clusters.[33] Following our previous work, the laser peak intensity attenuation by an assembly of clusters is given by[33]

$$dI_M/dz=-0.424\xi E_{mol}\rho_{mol}/\tau, \tag{12}$$

where z is the propagation direction of the laser beam, E_{mol} is the average ion energy (in keV) per molecule, and ξ is a numerical parameter that is determined by the ratio of electron energy released in cluster extreme inner/outer ionization and of ion (nuclei) kinetic energy released in CE. Estimates of ξ values were obtained from previous simulations,[33] with $\xi=1.15$ in the CVI domain ($R_0\ll R_0^{(I)}$), and $\xi=1.83$ in the far range of the non-CVI domain ($R_0\gg R_0^{(I)}$). For our calculations we took the value of $\xi=1.5$, which corresponds to $R_0\sim R_0^{(I)}$.

We shall take the light attenuation to be significant when the initial intensity decreases by 33%. The corresponding distances, denoted by $Z_{1/3}$, are presented in Fig. 5 for the size averaged ion energies (with $\sigma_n=1.0$). In the cylindrical filament with length Z_f, the decrease of the reaction yield due to light attenuation is taken to be negligible for $Z_{1/3}\geq Z_f$, whereas for $Z_{1/3}<Z_f$ the yield corrected for the attenuated laser peak intensity is approximately decreased by $(Z_{1/3}/Z_f)$, due to the reduction of the effective filament volume. In Fig. 5 we present the effect of light attenuation on the reaction yields for the filament volume of $V_f=5\times10^{-7}$ cm^3 used by us and for two values of the filament length: $Z_f=0.04$ and 0.02 cm. In Fig. 5 we also show data for the yields Y, with Y_{OF} providing the dominating contribution to nucleosynthesis. In contrast to Y_{IF}, which also decreases with increasing attenuation, Y_{OF} does not depend on the filament shape. For larger values of R_{av}, which are of interest to us, the decrease of the Y_{OF} yields due to light attenuation does not exceed the numerical factor of ~5.

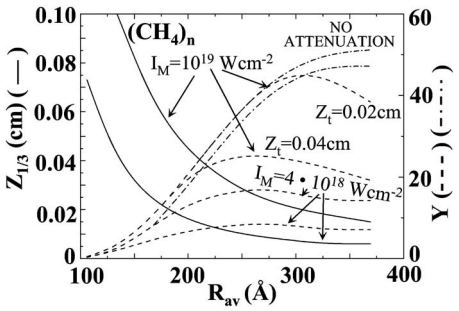

FIG. 5. Attenuation of a laser beam in an assembly of nanodroplets with $\rho_{mol}=4\times10^{18}$ cm^{-3}, size domain $R_{av}=100-400$ Å, peak intensities $I_M=4\times10^{18}$ W cm^{-2} and 10^{19} W cm^{-2}, for values of $Z_f=0.02$ cm and 0.04 cm (marked on the curves). The distances $Z_{1/3}$ for 33% attenuation of the incident intensity (——) decrease with decreasing the cluster size. The yields calculated with attenuation (- - - - -) are reduced relative to the yields without attenuation, decreasing with increasing Z_f, and increasing with increasing I_M.

From the foregoing analysis, we conclude that with the realistic nanodroplet beam and laser parameters used herein, and for a size dispersion width of $\sigma_n=1$, CE of methane clusters (nanodroplets) with $R_{av}>160$ Å driven by an ultraintense laser with $I_M\geq4\times10^{18}$ W cm^{-2} ($\tau=25$ fs) is ex-

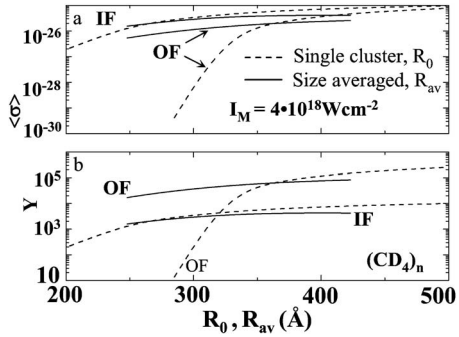

FIG. 6. Energy averaged and size averaged cross sections (upper panel) and nucleosynthesis yields per laser pulse (lower panel) for the $^{12}C(d,n)^{13}N$ reaction in the IF mode and in the OF mode, as marked on the curves. Single cluster (- - - - -) and size averaged (——) data were obtained at $I_M=4\times10^{18}$ W cm^{-2}.

pected to provide detectable nucleosynthesis yields in the range of 10–100 per laser pulse, which are amenable to experimental observation.

IV. NEUTRON YIELD FROM THE $^{12}C(d,n)^{13}N$ REACTION

We considered the $^{12}C(p,\gamma)^{13}N$ reaction driven by CE of methane $(CH_4)_n$ nanodroplets. Another nucleosynthesis process involving $^{12}C^{6+}$ nuclei is the $^{12}C(d,n)^{13}N$ reaction driven by CE of deuterated methane $(CD_4)_n$ nanodroplets. This reaction, which has not yet been studied experimentally in cluster beams, was recently subjected to an experimental study by Youssef *et al.*,[28] by the irradiation of a CD_2-solid target with a near-infrared laser and a peak intensity of $I_M=3\times10^{18}$ W cm^{-2}. The cross section for the $^{12}C(d,n)^{13}N$ reaction is relatively large, being about 2×10^{-25} cm^{-2} at maximum, with a high (~0.5 MeV) center of mass energy threshold.[36] Simulations of $(CD_4)_n$ cluster–ultraintense laser interactions were performed for the cluster size interval of 250 Å$<R_0<$500 Å at the laser peak intensity of $I_M=4\times10^{18}$ W cm^{-2}, which is close to the experimental value of $I_M=3\times10^{18}$ W cm^{-2}.[28] The energies of the light (D^+) and heavy (C^{6+}) ions produced by CE of $(CD_4)_n$ differ by <10% from the energies of the H^+ and C^{6+} produced by CE of $(CH_4)_n$ with the same size. In Fig. 6 we present our simulation results for the cluster size dependence of the reaction cross sections and the neutron yields calculated for the energy distribution for single clusters and for the size averaged energy distribution. These data were obtained using Eq. (2), with the $\langle\sigma\rangle$ values calculated from Eqs. (3)–(6) with E^H being replaced by the deuteron energy E^D, and m_H being replaced by the deuteron mass m_D and using the cross sections for the $^{12}C(d,n)^{13}N$ reactions.[36] The size-dependent energetic data were obtained from SEID MD simulations and from the size distribution parameter $\sigma_n=1$. The plasma filament parameters were taken to be identical to those used in Secs. II and III.

The energy averaged reaction cross sections $\langle\sigma\rangle$ and the neutron yields Y of single clusters increase monotonically with increasing R_0 (Fig. 6). This increase is much steeper in the IF mode than in the OF mode with $\langle\sigma\rangle_{IF}$ being larger than $\langle\sigma\rangle_{OF}$ in the entire R_0 interval, resulting in $Y_{IF}>Y_{OF}$ for smaller clusters and $Y_{OF}>Y_{IF}$ for larger clusters. The $\langle\sigma\rangle$ and Y values for cluster size averaged energy distributions are presented in Fig. 6, in terms of their dependence on the averaged cluster radii R_{av} (in analogy with Fig. 4). These $\langle\sigma\rangle$ and Y values increase with increasing R_{av}, with $Y_{OF}>Y_{IF}$ in the entire R_{av} interval. Thus, for a cluster size distribution, the OF mode dominates. For a large nanodroplet with $R_{av}=400$ Å, the size averaged yields provide $Y_{OF}/Y_{IF}=20$. In the size domain of large clusters ($R_{av}>300$–450 Å), the neutron yield Y_{OF} becomes large, being of the order of 5×10^4–9×10^4 per laser pulse. This estimate of the neutron yield for the $^{12}C(d,n)^{13}N$ reaction driven by CE explosion of $(CD_4)_n$ clusters ($R_{av}>300$–450 Å) is smaller by only a numerical factor of 4–7 than in the experimental results[28] for the yield of this nucleosynthesis reaction driven by laser (at similar intensity) – CD_2 solid interaction.

TABLE I. Scaled MD simulations of deuteron averaged and maximal energies and the cross sections in the OF mode for the $^{12}C(d,n)^{13}N$ reaction driven by CE of $(CD_4)_n$ nanodroplets.

R_0 (Å)	n	E^D_{av} (MeV)	E^D_M (MeV)	$\langle\sigma\rangle_{OF}$ (cm^2)
285	1.55×10^6	0.356	0.549	4.18×10^{-30}
326	2.41×10^6	0.456	0.709	7.85×10^{-27}
369	3.47×10^6	0.549	0.886	2.47×10^{-26}
423	5.27×10^6	0.667	1.130	5.04×10^{-26}
498	8.87×10^6	0.861	1.480	7.76×10^{-26}

The $^{12}C(d,n)^{13}N$ reaction studied herein competes with the $D(d,n)^3He$ fusion reaction, with neutron production in both channels.[28] In what follows we consider the cross sections and the product neutron energies of those two parallel reactions. In Table I we present the deuteron energies of CE of $(CD_4)_n$ nanodroplets, together with the corresponding energy averaged cross sections $\langle\sigma\rangle_{OF}$, for the $^{12}C(d,n)^{13}N$ reaction in the dominating OF mode. The energy averaged cross sections exhibit a four-orders-of-magnitude increase for CE of $(CD_4)_n$ nanodroplets in the size domain of $R_0=285$–370 Å, while high and weakly size dependent values of the cross sections $\sigma=2.5\times10^{-26}$–7.8×10^{-26} cm^2 are exhibited in the size domain $R_0=370$–500 Å, where $E^D_M=0.89$–1.48 MeV (Table I and Fig. 6), specifying the conditions for efficient CE driving of $^{12}C(d,n)^{13}N$ nucleosynthesis. On the other hand, the cross sections for the $D(d,n)^3He$ reaction vary weakly throughout the entire size and CE energy domain of Table I, rising from $\sigma=5\times10^{-26}$ cm^2 at $R_0=285$ Å ($E^D_M=0.55$ MeV) to $\sigma=9.6\times10^{-26}$ cm^2 at $R_0=500$ Å ($E^D_M=1.5$ MeV).[30] Accordingly, in the relevant energy range and nanodroplet size domain where the $^{12}C(d,n)^{13}N$ and $D(d,n)^3He$ reactions occur in parallel, their cross sections are comparable. Since the energy ratio $E^C_M/E^D_M=5$–6 is close to the mass ratio $m_C/m_D=6$, the contribution of the energetic ^{12}C nuclei to the $^{12}C(d,n)^{13}N$ reaction is similar to that of the energetic deuterons. Straightforward kinetic considerations indicate that for the OF mode with equal values of the cross sections, the relative yields for

the $^{12}C(d,n)^{13}N$ and $D(d,n)^3He$ reactions are $\sim 1/2$, so that the neutron yields for the two parallel reactions are of the same magnitude. However, the two reactions produce neutrons in different energy regions. We estimated the neutron energies produced by deuterons with an energy of 1.3 MeV, and ^{12}C nuclei with an energy of 7.8 MeV [driven by CE of $(CD_4)_n$ nanodroplets with $R_0=450$ Å and $I_M=4\times10^{18}$ W cm^{-2}], by using the analysis of Youssef *et al.*[28] The endothermic $^{12}C(d,n)^{13}N$ reaction ($^{12}C+D\rightarrow{}^{13}N+n-0.28$ MeV),[36] which has an energetic threshold for deuterons of 0.328 MeV, will result in neutrons in the energy range of up to 2.4 MeV.[28] On the other hand, the $D(d,n)^3He$ reaction ($D+D\rightarrow{}^3He+n+3.38$ MeV) with $E_M^D=1.3$ MeV will produce neutrons in the energy range of 2.3–4.5 MeV.[28] Neutron energy resolution will distinguish between the two parallel reaction channels, with lower energy (0–2.4 MeV) neutrons being produced by the $^{12}C(d,n)^{13}N$ reaction.

V. DISCUSSION

We explored the yields for the $^{12}C(p,\gamma)^{13}N$ and the $^{12}C(d,n)^{13}N$ nucleosynthesis reactions driven by high-energy CE of $(CH_4)_n$ and $(CD_4)_n$ nanodroplets ($n=10^4-10^7$, $R_0=100-500$ Å). Our computational-theoretical study of multielectron inner ionization, nanoplasma response, and outer ionization, as well as CE of nanodroplets, rests on the SEID MD simulation procedure, which provides the input information for the calculations of the nucleosynthesis reaction yields. At $4\times10^{18}-10^{19}$ W cm^{-2} ($\tau=25$ fs) and under realistic experimental conditions, the $^{12}C(p,\gamma)^{13}N$ nucleosynthesis driven by CE of $(CH_4)_n$ nanodroplets (with $R_{av}=250-350$ Å) is characterized by γ-ray yields (per laser pulse) of $Y\sim100$ in the absence of attenuation, reducing to $Y\sim20$ for effective laser beam attenuation. In the same intensity range, the $^{12}C(d,n)^{13}N$ nucleosynthesis driven by CE of $(CD_4)_n$ nanodroplets (with $R_{av}=300-450$ Å) is characterized by neutron yields of $Y\approx(4-9)\times10^4$ in the absence of attenuation. We conclude that table-top $p+{}^{12}C$ and $d+{}^{12}C$ nucleosynthesis driven by CE of molecular nanodroplets is amenable to experimental observation.

We advanced a theoretical and computational study of the conditions for the realization of an efficient target for nucleosynthesis with moderately heavy ^{12}C nuclei, driven by CE of $(CH_4)_n$ and $(CD_4)_n$ nanodroplets in ultraintense, near-infrared laser fields. For the $p+{}^{12}C$ and $d+{}^{12}C$ reactions, as well as for reactions involving other moderately heavy nuclei (i.e., $p+{}^{14}N$ or $p+{}^{16}O$),[24] experimental results are not yet available, whereupon the present study provides predictions for the attainment of nucleosynthesis driven by CE of nanodroplets under "real-life" conditions. The currently available relevant experimental results pertain to the $^{12}C(d,n)^{13}N$ fusion reaction driven by solid surface interactions[28] (Sec. IV), whose analysis is complicated by debris problems.[22] A central result emerging from our analysis of nucleosynthesis reactions with ^{12}C nuclei is the energetic requirement for the production of protons and deuterons with average and maximal energies in the range of 0.5–2 MeV, which is accomplished by CE of nanodroplets ($R_0=100-500$ Å). An experimental confirmation of our theoretical and computational results emerges from the production of deuterons in the energy range up to 1–2 MeV, which was reported by Ter-Avetisyan *et al.*[22] They used D_2O spray targets (with a nanodroplet radius of ~750 Å), driven by lasers at a peak intensity of 10^{19} W cm^{-2}. A heuristic, though satisfactory, comparison was obtained between the experimental results for maximal deuteron energies in CE of exploding $(D_2O)_n$ nanodroplets ($E_M^D=1.3\pm0.2$ MeV for $R_0\sim750$ Å at $I_M=10^{19}$ W cm^{-2}),[22] and our computational results for CE of $(CD_4)_n$ nanodroplets reported in Sec. IV (e.g., $E_M^D=1.48$ MeV for $R_0=500$ Å at $I_M=4\times10^{18}$ W cm^{-2}). In view of the variance between the C^{6+} and O^{8+} charges, and the differences (within a numerical factor of 2 or less) in the number of deuterons in the molecular constituents, the nanodroplet radii and the intensities, this comparison is only approximate. The realization of an efficient target of nanoparticles ($R_0>100$ Å) or clusters ($R_0<100$ Å) requires that CE of the extremely charged nanostructures will produce nuclei with sufficiently high kinetic energies for which the nuclear reaction cross sections attain high values. As pointed out in Ref. 22, the use of MeV deuterons for the $D(d,n)^3He$ reaction driven by CE of $(D_2O)_n$ nanodroplets is advantageous, as the cross sections increase from $\sigma=1.7\times10^{-26}$ cm^2 at $E_{cm}=100$ keV to $\sigma=9.6\times10^{-26}$ cm^2 at $E_{cm}=1$ MeV.[30] However, the moderate increase of σ in this energy range $E_M^D=100$ keV–1 MeV enables experimental studies of dd fusion driven by CE of deuterium containing clusters (in the size domain of $R_0=30-100$ Å) in the lower energy range of 120 keV,[21] and even at lower energies of $\sim10-120$ keV,[6,8,20–23] in accord with theoretical-computational results.[11,12,37] On the other hand, for the $^{12}C(d,n)^{13}N$ reaction driven by CE of $(CD_4)_n$ nanostructures (Sec. IV) at $I_M=4\times10^{18}$ W cm^{-2}, the energy averaged cross sections steeply rise (by four orders of magnitude) in the size domain $R_0=285-370$ Å and exhibit a moderate increase in the range $R_0=370-500$ Å (Table I and Fig. 6), while averaging over the nanodroplet size distribution will increase the size domain for this reaction (Fig. 6). Accordingly, it is imperative to use large nanodroplets ($R_0=200-500$ Å) for efficient $^{12}C(d,n)^{13}N$ nucleosynthesis. High-energy dynamics of multicharged nanostructures transcends dd fusion driven by keV CE of clusters towards nucleosynthesis with moderately heavy nuclei driven by MeV CE of nanodroplets.

An important mechanistic aspect of the nucleosynthesis reactions considered herein pertains to the distinction between the IF reaction mode within the laser focal volume and the OF reaction mode outside it. A cursory examination of the dependence of the ratio yields on the geometric factors of the laser+cluster beam [Eq. (2)] reveals that this ratio is independent of V_f, where $Y_{OF}/Y_{IF}\propto(\ell_{OF}/\ell_{IF})\langle\sigma\rangle_{OF}/\langle\sigma\rangle_{IF}$, with the radius of the cluster beam being $\ell_{OF}\simeq0.1$ cm, while $\ell_{IF}=1.6r_f\sim10^{-3}$ cm. In this size domain, where effective nucleosynthesis prevails ($R_0=300-450$ Å), the cross sections $\langle\sigma\rangle_{IF}$ and $\langle\sigma\rangle_{OF}$ are nearly equal, within a numerical factor of 2. Accordingly, for the experimental parameters used herein, $\ell_{OF}/\ell_{IF}\simeq30$, the OF mode is dominating in the intensity range of $I_M=4\times10^{18}-10^{19}$ W cm^{-2}. Regarding the $^{12}C(p,\gamma)^{13}N$ nucleosynthesis with $Y_{OF}/Y_{IF}\simeq100$, it is inter-

esting to inquire what the experimental implications of this result are, and whether it is possible to resolve the minority IF mode from the majority OF mode. A study of the dependence of $Y_{\mathrm{tot}}=Y_{\mathrm{IF}}(r_f)+Y_{\mathrm{OF}}$ on the plasma filament radius r_f, will be fraught with difficulties. The realization of distinct time scales for the IF and OF reaction modes will provide a new diagnostic tool for the identification of these different channels. Our analysis of the time scales for the IF and OF reaction modes for $^{12}\mathrm{C}(\mathrm{p},\gamma)^{13}\mathrm{N}$ nucleosynthesis will use the velocity $v=9.4\times10^{8}$ cm s^{-1}, corresponding to the energies $E^{\mathrm{H}}=460$ keV or $E^{\mathrm{C}}=2.76$ MeV at the maximum in $\sigma(E_{\mathrm{cm}})$ for this reaction (Fig. 1). In what follows, the time scales will be presented relative to the peak of the laser pulse (at $t=0$). For the IF mode, the temporal onset is at $t^{\mathrm{IF}}_{\mathrm{ONSET}}=(\tau+R_{\mathrm{Dr-Dr}}/v)$, where $\tau=25$ fs is the pulse width (which approximates the time for ion acceleration to the final CE velocity v). The distance between nanodroplets is $R_{\mathrm{Dr-Dr}}=(\bar{n}/\rho_{\mathrm{mol}})^{1/3}$, where $\rho_{\mathrm{mol}}4\times10^{18}$ cm^{-3} and $\bar{n}$ is the average number of molecules in the nanodroplet, with typical cluster sizes $\bar{n}=1.8\times10^{6}$ ($R_0=300$ Å), giving $R_{\mathrm{Dr-Dr}}=8\times10^{-5}$ cm. Accordingly, $t^{\mathrm{IF}}_{\mathrm{ONSET}}\approx65$ fs. The temporal end of the IF reaction mode is at $t^{\mathrm{IF}}_{\mathrm{END}}=\ell_{\mathrm{IF}}/v$, where $\ell_{\mathrm{IF}}=1.6r_f$ (see Sec. II A), so that $t^{\mathrm{IF}}_{\mathrm{END}}\simeq3$ ps. Thus, the interval scale for the IF mode falls in the range $\Delta t^{\mathrm{IF}}=65$ fs–3 ps. The time scale for the OF reaction mode is considerably longer than for the IF mode. The onset of the OF mode is $t^{\mathrm{OF}}_{\mathrm{ONSET}}=r_f/v\simeq2$ ps, while the temporal end of this mode is $t^{\mathrm{OF}}_{\mathrm{END}}=\ell_{\mathrm{OF}}/v\sim100$ ps. Thus, the time interval for the OF mode is $\Delta t^{\mathrm{OF}}=2-100$ ps, being by a numerical factor of ~30 longer than for the IF mode. Time-resolved γ-ray emission from the $^{12}\mathrm{C}(\mathrm{p},\gamma)^{13}\mathrm{N}$ reaction in exploding methane nanodroplets is expected to provide novel dynamic information on the reaction modes for tabletop nucleosynthesis driven by nanodroplet CE.

ACKNOWLEDGMENTS

This research was supported by the James-Franck Binational German-Israeli Program on Laser-Matter Interaction, and by the Deutsche Forschungsgemeinschaft (DFG) SFB 450 on "Analysis and Control of Ultrafast Photoinduced Reactions."

[1] I. Last and J. Jortner, Phys. Rev. A **62**, 013201 (2000).
[2] V. P. Krainov and M. B. Smirnov, Phys. Rep. **370**, 237 (2002).
[3] U. Saalmann, Ch. Siedschlag, and J. M. Rost, J. Phys. B **39**, R39 (2006).
[4] T. Ditmire, J. W. G. Tisch, E. Springate, M. B. Mason, N. Hay, R. A. Smith, J. Marangos, and M. H. R. Hutchinson, Nature (London) **386**, 54 (1997).
[5] E. Springate, N. Hay, J. W. G. Tisch, M. B. Mason, T. Ditmire, M. H. R. Hutchinson, and J. P. Marangos, Phys. Rev. A **61**, 063201 (2000).
[6] J. Zweiback, R. A. Smith, T. E. Cowan, G. Hays, K. B. Wharton, V. P. Yanovsky, and T. Ditmire, Phys. Rev. Lett. **84**, 2634 (2000).
[7] K. J. Mendham, N. Hay, M. B. Mason, J. W. G. Tisch, and J. P. Marangos, Phys. Rev. A **64**, 055201 (2001).
[8] K. W. Madison, P. K. Patel, D. Price, A. Edens, M. Allen, T. E. Cowan, J. Zweiback, and T. Ditmire, Phys. Plasmas **11**, 270 (2004).
[9] S. Zamith, T. Martchenko, Y. Ni, S. A. Aseyev, H. G. Muller, and H. J. J. Vrakking, Phys. Rev. A **70**, 011201(R) (2004).
[10] M. Hohenberger, D. R. Symes, K. W. Madison, A. Sumeruk, G. Dyer, A. Edens, W. Grigsby, G. Hays, M. Teichmann, and T. Ditmire, Phys. Rev. Lett. **95**, 195003 (2005).
[11] I. Last and J. Jortner, Phys. Rev. A **64**, 063201 (2001).
[12] I. Last and J. Jortner, J. Chem. Phys. **121**, 8329 (2004).
[13] J. Davis, G. M. Petrov, and A. L. Velikovich, Phys. Plasmas **13**, 064501 (2006).
[14] I. Last and J. Jortner, Phys. Rev. A **73**, 013202 (2006).
[15] A. Heidenreich, I. Last, and J. Jortner, Eur. Phys. J. D **35**, 567 (2005).
[16] I. Last and J. Jortner, Phys. Rev. A **75**, 042507 (2007).
[17] K. Nishihara, H. Amitani, M. Murakami, S. V. Bulanov, and T. Zh. Esirkepov, Nucl. Instrum. Methods Phys. Res. A **464**, 98 (2001).
[18] S. Sakabe, S. Shimizu, M. Hashida, F. Sato, T. Tsuyukushi, K. Nishihara, S. Okihara, T. Kagawa, Y. Izawa, K. Imasaki, and T. Iida, Phys. Rev. A **69**, 023203 (2004).
[19] H. Li, J. Liu, Ch. Wang, G. Ni, R. Li, and Zh. Xu, Phys. Rev. A **74**, 023201 (2006).
[20] S. Ter-Avetisyan, M. Schnürer, P. V. Nickles, M. Kalashnikov, E. Risse, T. Sokollik, W. Sandner, A. Andreev, and V. Tikhonchuk, Phys. Rev. Lett. **96**, 145006 (2006).
[21] G. Grillon, Ph. Balcou, J.-P. Chambaret, D. Hulin, J. Martino, S. Moustaizis, L. Notebaert, M. Pittman, Th. Pussieux, A. Rousse, J.-P. Rousseau, S. Sebban, O. Sublemontier, and M. Schmidt, Phys. Rev. Lett. **89**, 065005 (2002).
[22] S. Ter-Avetisyan, M. Schnürer, D. Hilscher, U. Jahnke, S. Bush, P. V. Nickles, and W. Sandner, Phys. Plasmas **12**, 012702 (2005).
[23] S. Karsch, S. Düsterer, H. Schwoerer, F. Ewald, D. Habs, M. Hegelich, G. Pretzler, A. Pukhov, K. Witte, and R. Sauerbrey, Phys. Rev. Lett. **91**, 015001 (2003).
[24] I. Last and J. Jortner, Phys. Rev. Lett. **97**, 173401 (2006).
[25] E. G. Adelberger, S. M. Austin, J. N. Bahcall *et al.*, Rev. Mod. Phys. **70**, 1265 (1998).
[26] I. Last and J. Jortner, J. Chem. Phys. **120**, 1336 (2004).
[27] G. M. Petrov, J. Davis, A. L. Velikovich, P. Kepple, D. Gasgupta, and R. W. Clark, Phys. Plasmas **12**, 063103 (2003).
[28] A. Youssef, R. Kodama, H. Habara, K. A. Tanaka, Y. Sentoku, M. Tampo, and Y. Toyama, Phys. Plasmas **12**, 110703 (2005).
[29] J. Zweiback, T. E. Cowen, R. A. Smith, J. M. Hartley, R. Howell, C. A. Stenke, G. Hays, K. B. Wharton, J. K. Crane, and T. Ditmire, Phys. Rev. Lett. **85**, 3640 (2000).
[30] D. D. Clayton, *Principles of Stellar Evolution and Nucleosynthesis* (McGraw-Hill, New York, 1968), p. 298.
[31] P. B. Parks, T. E. Cowan, R. B. Stephens, and E. M. Campbell, Phys. Rev. A **63**, 063203 (2001).
[32] M. R. Islam, U. Saalman, and J. M. Rost, Phys. Rev. A **73**, 041201 (2006).
[33] I. Last and J. Jortner, Phys. Rev. A **73**, 063201 (2006).
[34] *The Physical Encyclopedic Dictionary*, Soviet Encyclopaedia Vol. 4 (Russian Academy of Science, Moscow, 1965), p. 233 (in Russian).
[35] H. A. Bethe and J. Ashkin, in *Experimental Nuclear Physics*, edited by E. Segré (John Wiley & Sons, New York, 1960), p. 167.
[36] R. W. Mickelmann, J. Krauskopf, J. D. Meyer, and K. Bethge, Nucl. Instrum. Methods Phys. Res. B **51**, 1 (1990).
[37] A. Heidenreich, I. Last, and J. Jortner, Proc. Natl. Acad. Sci. U.S.A. **103**, 10589 (2006).